Decellularized liver hydrogel enhances cell engraftment in orthotopic hepatocyte transplantation by promoting cell–cell interaction and angiogenesis

Daisuke Udagawa
Keio University
Shogo Nagata
Keio University
Hiroshi Yagi (hy0624@gmail.com)
Keio University
Kotaro Nishi
Keio University
Toshinori Morisaku
Keio University
Shungo Adachi
National Institute of Advanced Industrial Science and Technology
Yutaka Nakano
Keio University
Masayki Tanaka
Keio University
Shutaro Hori
Keio University
Yasushi Hasegawa
Keio University
Yuta Abe
Keio University
Minoru Kitago
Keio University
Yuko Kitagawa
Keio University

Article

Keywords:

Posted Date: May 17th, 2023

DOI: https://doi.org/10.21203/rs.3.rs-2789456/v1

Abstract

Hepatocyte transplantation (HCT) is a potential bridging therapy or an alternative to liver transplantation. Conventionally, single-cell hepatocytes are injected via the portal vein. This strategy, however, has yet to overcome poor cell engraftment and function. Therefore, we developed an orthotopic hepatocyte transplantation method using a liver-derived extracellular matrix (L-ECM) gel. PXB cells (flesh mature human hepatocytes) were dispersed into the hydrogel solution in vitro, and the gel solution was immediately gelated in 37 ℃ incubators to investigate the affinity between mature human hepatocyte and the L-ECM-gel. During the 3-day cultivation in hepatocyte medium, PXB cells formed cell aggregates via cell–cell interactions. Quantitative analysis revealed human albumin production in culture supernatants. For the in vivo assay, PXB cells were encapsulated in the L-ECM gel and transplanted between the liver lobes of normal rats. Pathologically, the L-ECM gel was localized at the transplant site and retained PXB cells. Cell survival and hepatic function marker expression were verified in another rat model wherein thioacetamide was administered to induce liver fibrosis. Moreover, cell–cell interactions and angiogenesis were enhanced in the L-ECM gel compared to that in the collagen gel. Our results indicate that L-ECM gels can help engraft transplanted hepatocytes and express hepatic function as a scaffold for cell transplantation.

Introduction

Hepatocyte transplantation (HCT) has been explored as a less invasive therapy for patients with acute liver failure or metabolic liver diseases, with the potential to be a bridging therapy or an alternative to liver transplantation. HCT was first performed in a rat model of Crigler-Najjar syndrome in 1976. [1] Since the first attempt at HCT in a human patient with cirrhosis in 1992, [2] HCT has been performed in over 100 patients with the liver disease globally, with intraportal single-cell injection being the standard procedure. [3] Nevertheless, the therapeutic impact of intraportal HCT has been limited because of inadequate cell engraftment caused by cell emboli and instant blood-mediated inflammatory reactions. [4] [5] These impediments continue to hinder HCT from being used in the clinical setting.

To circumvent the difficulty of intraportal HCT, ectopic HCT of the spleen [6], subcutaneous spaces [7], lymph nodes [8], and intraperitoneal cavity [9] has been reported. Furthermore, scaffold biomaterials, including cell sheets and hydrogels, have gained prominence for ectopic HCT because of their ability to retain transplanted hepatocytes in space. [10] [11] [12] [13] These ectopic transplantations successfully maintain hepatic function. [14] However, the confinement of transplanted hepatocytes to the ectopic space limits cell–cell and cell–extracellular matrix (ECM) interactions inherent in the tissue-specific microenvironment of the liver. These organ-specific environments are essential for hepatocyte proliferation and the expression of inherent functions. [15] [16]

Many studies have demonstrated the method of orthotopic HCT coupled with biomaterials, such as cell sheets and patch grafts, as another approach to HCT. [17] [18] These studies reported contact between transplanted hepatocytes and the liver parenchyma of the recipient, as well as substantial cell

engraftment. Recently, biological scaffolds have piqued the interest of researchers because of their biocompatibility and bioactivity. [19] ECM hydrogels prepared by solubilizing decellularized tissues and removing cells and nucleic acid components are beneficial for cell culture [20]. They have been reported to promote the inherent functions of hepatocytes *in vitro* and *in vivo*. [21] [22]. Kidney-derived decellularized ECM hydrogels have also been reported to enhance vascularization. [23] [24]

In this study, we hypothesized that a decellularized liver hydrogel contributes to the survival of transplanted hepatocytes and the expression of their inherent functions via enhanced self-organization and vascularization. Here, we developed a liver-derived extracellular matrix (L-ECM) gel that functions as a scaffold material and investigated the orthotopic transplantation of mature hepatocytes in a fibrotic liver model. Our findings will help establish the therapeutic potential of L-ECM hydrogels as a scaffold for metabolic diseases, acute liver failure, and end-stage liver cirrhosis.

Results

Characterization of the L-ECM-gel

Figure 1A depicts the protocol for preparing the L-ECM gel via decellularization, lyophilization, pulverization, acidification, solubilization, neutralization, lyophilization, dilution, and gelation. Proteomic analysis revealed the components of the porcine liver and L-ECM gel, (See Fig. 1B.) indicating that the L-ECM gel contained liver-specific heterogeneous matrisomes and non-matrisomes. The matrisomes detected in the liver and L-ECM gel were mostly common, and liver-specific ECM components were retained (See Supplementary Fig. 1). Figure 1C depicts the ratio of ECM characteristics of the matrisome detected in the L-ECM gel via proteomic analysis. Type IV collagen has also been detected in some fibrotic proteins. Laminin also detected in some glycoproteins. A heat map of all matrisomes detected via proteomic analysis showed that several components, such as type IV and type I collagen, were more abundant in the L-ECM gel than in the liver itself. (Fig. 1D)

Evaluation of the proper viscoelasticity of the L-ECM-gel for hepatocytes in vitro **and** in vivo

The L-ECM gel was classified according to its viscoelasticity (n = 3), as shown in Fig. 2A. Electron microscopy revealed that the L-ECM gel had a structure similar to that of *in vitro* collagen fibers. (See Fig. 2B.) For both functional analysis and handling evaluation, HepG2 cells were cultured for 6 days in L-ECM gel according to viscoelasticity. Physical stability was achieved in a stiff L-ECM gel. In contrast, HepG2 cells did not survive in the stiff L-ECM gel. (See Fig. 2C.) In soft and intermediate L-ECM gels, HepG2 cells can survive and form a spheroid-like structure. However, soft gels are extremely fragile. Figure 2D depicts human albumin production in HepG2 cells as measured by ELISA. This was similar for the soft and intermediate L-ECM gels. Relative gene expression of hepatocyte markers and hepatic function, including *ALB, AFP, EPCAM*, and *HNF4α*, was similar between soft and medium L-ECM-gel (n = 3) (Fig. 2E). Based on these results, we determined that the proper viscoelasticity of the L-ECM gel for *in vivo* experiments was the intermediate. Immunohistochemistry analysis of HepG2 cells within

intermediate L-ECM-gel demonstrated that HepG2 cells expressed the hepatocyte marker (CK8) and hepatic function (HNF4α and albumin) within L-ECM-gel, rich in collagen IV. (See Fig. 2F).

Functional and histological analyses of the L-ECM and collagen gels as scaffold for hepatocytes in vitro

The functional and histological findings of PXB cells encapsulated in L-ECM gel were compared to those in collagen gel *in vitro*. (See Fig. 3A.) The intermediate viscoelasticity of the L-ECM gel was employed for *in vitro* analysis. PXB cells were cultured for three days before being characterized on the last day. Figure 3B depicts macroscopic changes in hepatocytes cultivated in L-ECM gel between days 0 and 1, indicating cell aggregation in the L-ECM gel. Human albumin production was similar between the two hydrogels in quantitative enzyme-linked immunosorbent assay (ELISA) (L-ECM gel, n = 7; collagen gel, n = 5), as shown in Fig. 3C. Immunohistochemistry analysis of PXB cells within L-ECM-gel demonstrated that PXB cells expressed the hepatocyte marker (CK8), hepatic function (HNF4α and albumin), and intercellular adhesion marker (E-Cadherin) within L-ECM-gel, rich in collagen IV. (See Fig. 3D). Relative gene expression analysis revealed that hepatocyte markers and PXB-cell hepatic function were not significantly different between the L-ECM gel and collagen gel; however, CYP3A4 expression was reduced in the L-ECM gel without significant difference ($P < 0.10$). The expressions of cell–cell interaction markers, such as *CLDN1* and *CLDN4*, and Yes-associated protein (YAP) pathways, such as CCN2 and CCN1, were increased in the L-ECM-gel with statistically significant differences (See Fig. 3E). RNA sequencing was performed to investigate the gene behavior of PXB-cell in two hydrogels: L-ECM and collagen gels. The volcano plot revealed that the expression of ALB, HNF4α, and EPCAM in PXB cells was not different in the L-ECM gel and collagen gel, as well as in the PCR data. In addition, the expressions of hepatic function markers such as CYP3A4 and UGT1A were downregulated in the L-ECM gel compared with that in the collagen gel. In contrast, the expressions of markers related to endothelial-to-mesenchymal transition (EMT) such as TWIST2, LOX, and SNAIL were upregulated in the L-ECM gel (See Supplementary Fig. 1A.). Moreover, gene set enrichment analysis (GSEA) demonstrated that the expressions of SMAD2 and SMAD4, downstream genes of the YAP pathway, and EZH2, an EMT-related gene, were significantly enriched in L-ECM-gel, whereas those of liver-specific genes were significantly reduced. (See Supplementary Fig. 1B.) Fig. 3F displays the gene sets of mature hepatocyte, ENT, partial EMT, and related angiogenesis of PXB cells encapsulated in hydrogels (L-ECM gel; n = 3, collagen gel; n = 1) using RNA sequencing. A gene set of mature hepatocytes, including *CYP3A4* was downregulated in the L-ECM gel. The gene set of EMT, such as *SNAI2* and *TGFBI*, was partially upregulated in L-ECM-gel. Moreover, the gene set of partial EMT- and angiogenesis-related genes was upregulated in the L-ECM gel. Gene ontology (GO) enrichment analysis revealed that cell–cell signaling, growth factor activity, and integrin complexes were enhanced in the L-ECM-gel. (See Fig. 3G)

Hepatocyte transplantation with the L-ECM-gel as a scaffold

PXB cells were embedded in L-ECM gel and transplanted onto the liver lobes of SD rats. The surgical procedure is illustrated in Fig. 4A. These procedures enabled the PXB cells embedded in L-ECM gel to

remain on the liver surface. The perioperative management is described in Fig. 4B. As an immunosuppressive control, splenectomy was performed during transplantation, and dual immunosuppressive agents, FK506 and methylprednisolone, were administered daily. One week after transplantation, native livers were sampled (n = 5). In the quantitative analysis, human albumin was detected in rat blood by ELISA and increased linearly after transplantation. (See Fig. 4C) Macroscopic findings demonstrated that the L-ECM gel was sandwiched in the liver lobes one week after transplantation (See Fig. 4D). Hematoxylin and eosin (H&E) staining revealed that the L-ECM-gel contained cells (See Fig. 4E). The L-ECM gel remained in the transplanted site and contained PXB (human albumin-positive) cells (See Fig. 4F). Moreover, CLAUDIN-1 expression was detected in PXB, indicating that cell–cell interactions exist in PXB encapsulated in L-ECM-gel. These results suggest that PXB survived in the L-ECM gel and expressed inherent hepatic function.

Protocol for constructing a thioacetamide (TAA)-induced liver fibrosis model of wild rat

A rat model of liver fibrosis was developed by administering TAA to evaluate cell engraftment in the damaged liver. TAA (100 mg/kg) was administered three times per week subcutaneously. This administration was scheduled for eight weeks (See Fig. 5A). No rats died during the study (TAA: n = 5; control: n = 6). Serum levels of AST and ALT were slightly elevated in the TAA group than in the control group without significant difference, and serum levels of albumin gradually reduced in the TAA group than in the control group without significant difference (See Fig. 5B). After the 8-week administration, the rat livers were analyzed. Histological analysis of the liver revealed that the TAA group presented a cross-linked structure, as seen using H&E and azan staining (Fig. 5C). According to the New Inuyama classification of liver fibrosis [25], the TAA group was matched for F2 (63%) and F1 (13%). qRT-PCR analysis of the liver revealed that the expression of inflammation-associated genes, including *IL1 and IL2; MMP; Col;* liver regeneration–associated genes, including *Fgf2* and *Pdgfa;* and ECM-associated genes, including *Mmp1* and *Col1a1*, was significantly elevated in the TAA group (See Fig. 5D).

Hepatocyte transplantation with the L-ECM-gel as a scaffold in the rat model of liver fibrosis

Cirrhotic liver induces portal hypertension, which negatively affects hepatocyte injection via the portal vein. Thus, the indications for intraportal HCT are limited. This study aimed to investigate the engraftment of transplanted hepatocytes in a damaged liver. Figure 6A shows the fibrotic liver induced by TAA administration during HCT. One week after transplantation, the rats were sampled (n = 3). L-ECM gel was observed on the surface of the liver lobes by HE and Azan staining (Fig. 6B). HE staining revealed red blood cells in the L-ECM gel. Azan staining demonstrated that the L-ECM gel had migrated to the native liver. Human albumin production was detected in blood samples using quantitative ELISA (See Fig. 6C). Relative gene expression was compared between the L-ECM gel and collagen gel. Hepatic function

markers, such as *CYP3A4*, and hepatocyte markers, such as *EPCA, KRT7*, and *LKB1*, were not significantly different between the two hydrogels. EMT markers, such as *CCN1*, and *CCN2*, were likewise similar in the two hydrogels. *CLDN1* and *CLDN3* expression did not differ significantly between the two hydrogels. Moreover, ABCB11 expression, a cholangiocyte marker, did not differ between groups (See Fig. 6D). In immunostaining analyses, PXB cells (CK8/18 and human albumin positive) exhibit an expression of hepatic function markers, including CYP3A4 (See Fig. 6E). Moreover, ZO-1, a marker of tight junctions, was detected in the L-ECM gel. Claudin-1 expression was detected in these cells. The rate of Claudin-1 positive area in the hydrogel was significantly higher in the L-ECM gel than in the type I collagen gel using ImageJ software (See Fig. 6F). Further evaluation of angiogenesis in the hydrogels was performed. Gene expression of *Pecam1* was significantly elevated in the L-ECM gel (Fig. 6G). Figure 6H shows that a vascular structure appeared in the L-ECM gel. Pecam1-positive areas were compared between L-ECM-gel and type I collagen gels using ImageJ software. The rate of Pecam1 positive area in the hydrogel was significantly higher in the L-ECM gel than in the type I collagen gel. (Fig. 6H)

Discussion

This study demonstrated the short-term cell engraftment of orthotopic HCT in combination with a L-ECM gel as a scaffold. Our orthotopic HCT method revealed the following: (i) survival of translated hepatocytes and expression of their inherent function in a rat model of drug-induced liver fibrosis, (ii) enhancement of the cell–cell interaction of transplanted hepatocytes, and (iii) induction of angiogenesis in the L-ECM-gel. These results suggest that the L-ECM gel can contribute to cell engraftment and the expression of their functions by promoting cell–cell interactions and angiogenesis in transplanted hepatocytes.

ECM hydrogels derived from decellularized tissues are encouraging materials for *in vitro* and *in vivo* cell bioengineering. [20] Various studies have reported that organ-specific ECM, including hepatocytes, works on cell function and proliferation [26] [27] [28]. [21] [29] Proteomic analysis revealed that matrisome, an essential component of ECM, [30] [31] is retained after decellularization. L-ECM-gel contains various important hepatocyte components, including Type IV collagen, laminin, and glycoproteins. [32] [33] Because the viscoelasticity of hydrogels is closely related to tissue homeostasis and regeneration, [34] [35] we investigated the proper viscoelasticity of L-ECM gel for cell function and applicable staff for surgical situations. Viscoelasticity can be adjusted in a concentration-dependent manner. *In vitro* quantitative analyses demonstrated that the production of albumin by mature hepatocytes was similar in the L-ECM gel and collagen gel. In vivo, L-ECM-gel can provide a physically stable scaffold for cell engraftment and the expression of its inherent function.

To investigate cell engraftment in our orthotopic HCT in a fibrotic liver, we generated a rat model of liver fibrosis by the subcutaneous administration of TAA. While Immunostaining analysis showed a fibrotic liver, TAA administration did not cause a significant increase in ALT and AST levels. No deaths occurred during this study. These results suggest that our method can be safely performed using the duplicate clinical features of cirrhotic livers. We used HCT in this TAA-induced liver fibrosis rat model, as well as in

normal rats. Currently, liver transplantation is the only life-saving treatment available for patients with cirrhosis. The shortage of donor livers has not yet been resolved, resulting in many patients on transplant waiting lists and a significant proportion dying before waiting [36] [37]. In the conventional method, injected hepatocytes are unable to reach the cirrhotic liver owing to the negative effect of portal hypertension. [38] This limits the indication for HCT in non-cirrhotic livers, such as those with metabolic disease. [4] Thus, our HCT method has the potential to be a bridging therapy for liver transplantation in patients with decompensated cirrhosis.

Gene expression analysis showed that *ALB* and *EPCAM* were retained in hepatocytes encapsulated in the L-ECM gel compared with those in the collagen gel *in vitro*. In contrast, in the L-ECM gel, the cluster gram of mature hepatocytes was downregulated, and that of EMT was upregulated compared with that in the collagen gel. Therefore, we performed a further subgroup analysis of partial EMT, which was upregulated. EMT is integral to the development and associated with wound healing, fibrosis, cancer progression, and stem cell differentiation. [39] In particular, partial EMT is necessary for hepatocyte regeneration. [40] [41] These gene behaviors of hepatocytes in L-ECM gel *in vitro* indicated that mature hepatocytes do not show a mesenchymal shift to fibroblasts but present the process of regeneration in such a liver-specific environment. In the analysis of transplanted hepatocytes in L-ECM gel *in vivo*, the expression of mature hepatocyte markers, such as *CYP3A4* was similar to that in the collagen gel, and ALB was significantly promoted. In addition, the expression of *CCN1* and *CCN2* associated with the YAP pathway, in the L-ECM gel was not statistically significantly different from that in the collagen gel. These results demonstrate that the transplanted hepatocytes are regulated as the epithelial phenotype *in vivo*. [42] As reported in previous studies, [14] [15] hepatocytes require cell–cell and cell–ECM interaction to survive for long time and express their inherent function. CLDN-1 and ZO-1 are essential cell surface proteins involved in cell–cell interactions and tight junctions. [43] [44] Immunostaining demonstrated that the CLDN-1 was strongly expressed in intercellular space and the area of CLDN-1 positives was significantly larger in L-ECM-gel than in collagen gel. This suggests that transplanted hepatocytes show an epithelial transition to regenerate in vivo and inherent hepatic function with promoted cell–cell interactions.

Moreover, angiogenesis was observed in the L-ECM gel. Cells and tissues require an oxygen supply and metabolite excretion routes. Mature hepatocytes have high demand on oxygen for survival. [45] [46] Thus, angiogenesis is a crucial issue in tissue engineering. [47] In this method, transplanted hepatocytes do not receive a direct blood supply, unlike in intraportal HCT. The RNA-sequence of hepatocytes demonstrated that the cluster gram of angiogenesis-related genes had higher expression in the L-ECM gel than in the collagen gel. *In vivo* histological analysis demonstrated the presence of red blood cell in the CD31-positive vascular structure in the L-ECM gel from the peel-off surface. These results indicated that the L-ECM gel has the potential to achieve long-term survival of transplanted hepatocytes by promoting angiogenesis. (See Supplementary Fig. 2).

In this study, we aimed to investigate the engraftment of mature hepatocytes in rats with normal livers and a rat model of liver fibrosis using a new orthotopic HCT approach. Although further investigation of the therapeutic effect and long-term outcomes of this HCT approach is necessary, our study

demonstrated that L-ECM gels contribute to the engraftment of transplanted mature hepatocytes by promoting cell–cell interaction and angiogenesis. We conclude that orthotopic hepatocyte transplantation with L-ECM hydrogels as a scaffold has clinical therapeutic potential for metabolic diseases, acute liver failure, and decompensated cirrhosis.

Methods

Animals

Adult female Sprague-Dawley rats between 8 and 16 weeks of age (weighing approximately 180–250 g) were used for all gel implantation experiments. All rats were bred ad libitum in a room at 24–25°C, 40–70% humidity, and 12 h of light and dark. All the experiments were approved by the Institutional Animal Care Committee. The experimental procedures and protocols were approved by the Animal Ethics Committee of Keio University Tokyo, Japan, (approval number: A2022-229) and were performed according to the Guide for the Care and Use of Laboratory Animals (National Institutes of Health, Bethesda, MD, USA). The animal experiments were performed according to the ARRIVE (Animal Research: Reporting of In Vivo Experiments) guidelines 2.0 as a guideline for animal experiments, and all necessary checklist criteria were met.

Human hepatocytes

HepG2 and PXB cells were obtained from Cellular Engineering Technologies, Inc., and Phoenix Bio, Japan, respectively. PXB cells are pure human hepatocytes freshly isolated from PXB mice that have been used in some *in vitro and in vivo* studies. [48] [49] For HepG2 culture, HepG2 Hepatocellular Carcinoma Expansion Media were used. PXB cells were cultured in 6-well culture plates according to the manufacturer's instructions.

Decellularization of porcine liver

The L-ECM was prepared according to a previous report, with some modifications [24] [50]. Briefly, livers were removed from the disinfected peritoneal cavity of pigs, frozen at − 80°C, and thawed at 4°C for over 24 h for the freeze-thaw process, a common initial decellularization step. The porcine liver was cut into small pieces using the food dicer DC-203 (Emura Food Machine CO, LTD, Japan) for uniform tissue decellularization. The fragments were then rinsed three times a day for two days at 4°C with phosphate-buffered saline (PBS; Fujifilm Wako Pure Chemical Inc., Osaka, Japan) under constant stirring. Thereafter, the fragments were decellularized with 1% TritonX-100 (Sigma-Aldrich Co., Tokyo, Japan) and ammonium hydroxide under continuously stirring for 5 days. To remove the remaining detergent, the pieces of decellularized liver were rinsed with PBS; the solution was changed thrice per day for 2 days. The pieces were then mixed with PBS containing an antibiotic, an antimycotic (Thermo Fisher Scientific K.K., Tokyo, Japan), and 300 μg/mL sodium colistin methanesulfonate (Fujifilm Wako Chemicals, Osaka, Japan) for

1 h, followed by the addition of PBS containing 1× antibiotic-antimycotic (Nacalai Tesque Co., Ltd., Tokyo, Japan) and 200 μg/mL gentamicin sulfate (Nacalai Tesque Co., Ltd., Tokyo, Japan) for 1 h. Decellularized liver ECM (dECM) powder was produced after 3 days of lyophilization and subsequent milling.

Hepatocyte cultivation in hydrogel

Cultured PXB and HepG2 cells were individually dissociated using Accutase (Thermo Fisher Scientific, USA) and mixed with the gel solution. In total, 8.0×10^5 human hepatocyte cells (PXB or HepG2) were encapsulated within the solution of 40 μL and 200 μL of either the L-ECM gel or the collagen gel. For PXB cells, a dimpled parafilm substrate was prepared for generating L-ECM gel droplets by layering a square of parafilm over an empty tip tray for 200-μL tips. [51] After immediate gelation in an incubator for 10 min, 3D culture was performed on the medium. After 3–6 days, the ELISA and qRT-PCR results of the supernatant and histological findings of the cells and hydrogel were analyzed. The PXB cells were encapsulated in hydrogel and grown for 3 days in Corning's ultra-low attachment 6-well plates.

Protein analysis

To analyze the samples, each sample was first digested and peptised in a solution containing 0.001% trypsin, 10 μM Tris-HCl, 0.005% n-octyl glucopyranoside, and 0.7 M guanidine hydrochloride (pH 8.8) for 12 hours. Subsequently, the resulting peptides were reduced with 5 mM tris(2-carboxyethyl) phosphine for 30 minutes at 65°C and alkylated with 10 mM iodoacetamide for 30 minutes at 25°C. The resulting digested peptides were then subjected to analysis using an Evosep One LC system (EVOSEP) connected to a Q-Exactive HF-X mass spectrometer (Thermo). The mobile phases consisted of 0.1% formic acid as solution A and 0.1% formic acid/99.9% Acetonitrile as solution B. The analysis was performed in data-dependent acquisition mode, and the top 25 recorded mass spectrometry spectra between 380 and 1500 m/z were selected for further analysis. All MS/MS spectra were then searched against the protein sequences of the Sus scrofa (NCBI: txid9823) protein database using Proteome Discoverer 2.2 with the SEQUEST search engine. The peptide spectrum match was subjected to a false discovery rate (FDR) set at 1% for reliability. To generate a heat map of the matrisomes identified via LC-MS, GraphBio was used.

Electron microscopy

The resulting organ-derived hydrogel solution was placed onto a glass slide, and the solution was transferred to the gel under the same conditions as described above. The L-dECM gel was fixed on a glass slide in a freshly prepared 2.5% glutaraldehyde solution for scanning electron microscopy. Samples were fixed with 1.0% osmium tetroxide (TAAB Laboratories) for 2 h at 4°C, rinsed in 0.1 M phosphate buffer (pH 7.4, Muto Pure Chemicals), and then treated with a series of escalating ethanol concentrations.

The samples were coated with osmium to a thickness of approximately 2 nm using a conductive osmium coater after being dried using a critical point drier (CPD300, Leica Biosystems; Neoc-ST, Meiwafosis). Using an SU6600 (Hitachi High Tech) apparatus, scanning electron microscopy images were captured at 5 keV.

Rheological characterization

The collagen concentration in the matrix gel solution was measured for each L-dECM concentration (8, 12, 16, and 20 mg/kg).

Using a longitudinal vibration viscoelastic meter (PZ-Rheo NDS-1000, Taisei Co., Ltd., Japan), the rheological characteristics of the L-dECM and rat tail collagen I hydrogels (Corning) were assessed. The samples were tested at 25°C with a fixed frequency of 3 Hz and an amplitude of 250 m to determine the dynamic viscosity. Compression tests were used to determine the storage modulus. Samples were measured using a 10-mm diameter parallel plate at 25°C with a fixed frequency of 3 Hz and an amplitude of 10 μm.

The rheological characteristics of the solubilized LCM gel were investigated using the same setting. In the linear regime, the hydrogel's total resistance to deformation was assessed by the complex viscoelastic modulus (E* = E' + iE"), where E' represented the storage modulus and E" represented the loss modulus. Moreover, Tan Delta (= E"/E') represented the hydrogel's frictional dissipations.

PXB transplantation

SD rats were used for the in vivo experiments. Figure 4A depicts the surgical procedures. After the incision, a splenectomy was performed. The left lateral lobe was mobilized to the median. Suturing of the lateral left, right, and internal left lobes with 3 – 0 vicryl was performed, and a pocket was made. Peeling of the bottom of the pocket on the lateral left lobe with Biopsy trepan large diameter type 12 mm (Kai Corporation, Japan). Subsequently, 8.0×10^5 cells of PXB embedded in the 40 μL of L-ECM gel was transplanted onto the pocket. In the rat model of liver fibrosis, 2 sets of 8.0×10^5 cells of PXB embedded in the 40 μL of L-ECM gel were translanted. PXB cells were cultured in L-ECM gel for 3 days before transplantation. Finally, suturing with lobes was performed, and the gel was packed into the liver lobes.

Postoperative management

Immunosuppressive agents were administered daily after transplantation. According to the protocol [52], PSL 20 mg/kg was administered intramuscularly and tacrolimus 1μg/kg was administered intrasubcutaneously. Ceftriaxone (20 mg/kg), an antibiotic, was administered daily for one week. The rats were sampled one week after transplantation. The postoperative schedule is shown in Fig. 4B.

Biochemical blood examination

Via the rat's subclavian vein, 500 µL of blood was taken. Biochemical analysis was performed with 100 µL by Piccolo Xpress (CENTRAL SCIENTIFIC COMMERCE, INC, JAPAN). The remaining blood was used for ELISA.

Gene expression analysis

Using an RNeasy Plus Mini Kit, total RNA was extracted from HepG2 and PXB cells (Qiagen, USA). A QuantiTect Rev was used to create cDNAs from 500 ng of total RNA for RT-PCR. Transcription Kit (Qiagen, USA) was used as directed by the manufacturer. SYBR Master Mix was used for the PCR (Thermo Fisher Scientific, USA). The Supplementary Table 1 contains the primer sequences. Rhelixa, Inc. carried out RNA sequencing (RNA-seq) for the whole-transcriptome study (Tokyo, Japan). Briefly, library construction was performed using NEBNext® Ultra™ II Directional RNA Library Prep Kit (Illumina), according to the manufacturer's instructions. Using the Illumina NovaSeq 6000 platform, sequencing was carried out. The expression profiles were derived as read counts and fragments per kilobase of transcripts per million mapped reads for each sample, transcript, and gene. The Benjamini–Hochberg approach was also used to identify differentially expressed genes (DEGs) using criteria of |log2 (Fold Change, FC)| > 1 and p-value 0.05. Using ggVolcanoR, a volcano graphic was produced using the FC and p-value of the DEGs. Using GraphBio, heatmaps were produced using the Z-scores of the normalized numbers. GOATOOLS (version 1.1.6) was used for GO analysis of DEGs, whereas ClusterProfiler was used for GSEA (Version 3.12.0).

Protein ELISA

The amounts of human ALB in the culture media and rat blood samples were assessed using a Human ALB ELISA Kit (Bethyl Laboratories, Inc.). On day 3, an ELISA kit was used to assess the level of human ALB in the culture media. On days three, five, and seven after transplantation, rat blood was collected.

Histological analysis

With 4% paraformaldehyde for 48 hours, harvested livers were fixed. The sections were cut to a thickness of 0.3 µm after being immersed in paraffin blocks. The sections were embedded in paraffin blocks and subsequently sliced into 0.3 µm thickness. Sections were stained with either azan or H&E (Sigma-Aldrich Co.) according to established procedures. Using a BZ-X800 microscope, the slides were captured as images (KEYENCE Co., Osaka, Japan).

Immunohistochemical analysis

The slices with paraffin embedding were deparaffinized and rehydrated. Citrate buffer (Dako, Agilent Technologies Japan, Ltd.) was used to extract the antigens from each segment for 15 minutes at 120°C.

The sections were treated with a primary antibody solution at 4°C overnight after blocking with 1% BSA (Sigma-Aldrich Co.). The primary antibodies and dilutions are as follows: anti-CK8/18 (P05786, Progen Bio), anti-human-albumin (ab10241, abcam), anti-claudin-1 (13255, Cell Signaling Technology), anti-E-cadherin (ab76055, abcam), anti-Collagen IV (ab6586, abcam), anti-HNF 4α (3113S, CST), ani-Pcam1 (ab182931, abcam), anti-human mitochondria (Merck, MAB1273), anti-DPP IV (CST, 40134S), anti-ZO-1 (Invitrogen, 33-9100), and anti-integrin (abcam ab52971) antibodies and laminin (ab11575, Abcam).

After rinsing, the pieces were mounted with DAPI and ProLong Diamond Antifade Mountant (Invitrogen Inc., Carlsbad, CA, USA). Slides were imaged using a BZ-X810 microscope (KEYENCE Co., Osaka, Japan). Claudin-1 positive or Pcam1-positive areas were counted using ImageJ. Three samples were randomly chosen and claudin-1 or Pcam1 positive area were counted under the same conditions (range, threshold).

Statistical analysis

Paired continuous data were evaluated using Student's t-test. Statistical significance was defined as a p-value < 0.05. SPSS software (SPSS 28.0, Chicago, IL, USA) was used for the statistical analysis.

Declarations

Acknowledgements

This study was supported by grants from the Japan Agency for Medical Research and Development (AMED; 22bm1004003h0003), and a Grant-in-Aid for Challenging Research (Pioneering) (22K18395) awarded to H.Y. The authors thank S. Mizutani, K. Zhao, M. Ohtomo, and M. Takahashi for technical laboratory support.

Author contributions

Conceptualization, H. Y.; methodology, D. U., S. N., K. N., and H. Y.; investigation, D. U., S. N., and K. N.; proteomic analysis, D. U., S. N., and S. A.; writing—original draft preparation, D. U.; writing—review and editing, H. Y., S. N., T. M., S. A., M. T., S. H., Y. H., Y. A., K. M., and Y. K.; supervision, H. Y. and Y. K.; project administration, H. Y.; funding acquisition, H. Y. All authors have read and agreed to the published version of the manuscript.

Competing interests

The authors declare no competing interests.

Data availability statement

All raw sequencing data has been deposited in DDBJ Sequence Read Archive (DRA) database that is publicly accessible with bioproject accession number PRJDB15729.

References

1. Matas, A. J. *et al.* Hepatocellular transplantation for metabolic deficiencies: decrease of plasms bilirubin in Gunn rats. *Science* 192, 892–894 (1976). 10.1126/science.818706, Pubmed: 818706.
2. Mito, M., Kusano, M. & Kawaura, Y. Hepatocyte transplantation in man. *Transplant. Proc.* 24, 3052–3053 (1992). 10.1177/096368979300200109, Pubmed: 1466053.
3. Gramignoli, R., Vosough, M., Kannisto, K., Srinivasan, R. C. & Strom, S. C. Clinical hepatocyte transplantation: practical limits and possible solutions. *Eur. Surg. Res.* 54, 162–177 (2015). 10.1159/000369552, Pubmed: 25633583.
4. Iansante, V., Mitry, R. R., Filippi, C., Fitzpatrick, E. & Dhawan, A. Human hepatocyte transplantation for liver disease: current status and future perspectives. *Pediatr. Res.* 83, 232–240 (2018). 10.1038/pr.2017.284, Pubmed: 29149103.
5. Gustafson, E. K. *et al.* The instant blood-mediated inflammatory reaction characterized in hepatocyte transplantation. *Transplantation* 91, 632–638 (2011). 10.1097/TP.0b013e31820ae459, Pubmed: 21289595.
6. Andersson, A., Eriksson, U., Petersson, B., Reibring, L. & Swenne, I. Failure of successful intrasplenic transplantation of islets from lean mice to cure obese-hyperglycaemic mice, despite islet growth. *Diabetologia* 20, 237–241 (1981). 10.1007/BF00252634, Pubmed: 6785138.
7. Sakata, N. *et al.* Strategy for clinical setting in intramuscular and subcutaneous islet transplantation. *Diabetes. Metab Res. Rev.* 30, 1–10 (2014). 10.1002/dmrr.2463, Pubmed: 24000195.
8. Fontes, P., Komori, J., Lopez, R., Marsh, W. & Lagasse, E. Development of ectopic livers by hepatocyte transplantation into swine lymph nodes. *Liver Transpl.* 26, 1629–1643 (2020). 10.1002/lt.25872, Pubmed: 32810371.
9. Weber, C. J., Hardy, M. A., Lerner, R. L., Felig, P. & Reemtsma, K. Hyperinsulinemia and hyperglucagonemia following pancreatic islet transplantation in diabetic rats. *Diabetes* 25, 944–948 (1976). 10.2337/diab.25.10.944, Pubmed: 135703.
10. Baimakhanov, Z. *et al.* Efficacy of multilayered hepatocyte sheet transplantation for radiation-induced liver damage and partial hepatectomy in a rat model. *Cell Transplant.* 25, 549–558 (2016). 10.3727/096368915X688669, Pubmed: 26224253.
11. Kano, K., Yamato, M. & Okano, T. Ectopic transplantation of hepatocyte sheets fabricated with temperature-responsive culture dishes. *Hepatol. Res.* 38, 1140–1147 (2008). 10.1111/j.1872-034X.2008.00371.x, Pubmed: 18513332.
12. Török, E. *et al.* Primary human hepatocytes on biodegradable poly(l-lactic acid) matrices: a promising model for improving transplantation efficiency with tissue engineering. *Liver Transpl.* 17, 104–114 (2011). 10.1002/lt.22200, Pubmed: 21280182.
13. Yamada, K. *et al.* An improved encapsulation method for cryopreserving hepatocytes for functional transplantation using a thermo-reversible gelation polymer. *In Vivo* 34, 2309–2316 (2020). 10.21873/invivo.12043, Pubmed: 32871755.

14. Ohashi, K. *et al.* Engineering functional two- and three-dimensional liver systems in vivo using hepatic tissue sheets. *Nat. Med.* 13, 880–885 (2007). 10.1038/nm1576, Pubmed: 17572687.
15. Zaret, K. S. Liver specification and early morphogenesis. *Mech. Dev.* 92, 83–88 (2000). 10.1016/s0925-4773(99)00326-3, Pubmed: 10704889.
16. Si-Tayeb, K., Lemaigre, F. P. & Duncan, S. A. Organogenesis and development of the liver. *Dev. Cell* 18, 175–189 (2010). 10.1016/j.devcel.2010.01.011, Pubmed: 20159590.
17. Nagamoto, Y. *et al.* Transplantation of a human iPSC-derived hepatocyte sheet increases survival in mice with acute liver failure. *J. Hepatol.* 64, 1068–1075 (2016). 10.1016/j.jhep.2016.01.004, Pubmed: 26778754.
18. Zhang, W. *et al.* Patch grafting, strategies for transplantation of organoids into solid organs such as liver. *Biomaterials* 277, 121067 (2021). 10.1016/j.biomaterials.2021.121067, Pubmed: 34517276.
19. Zhang, X. *et al.* Decellularized extracellular matrix scaffolds: recent trends and emerging strategies in tissue engineering. *Bioact. Mater.* 10, 15–31 (2022). 10.1016/j.bioactmat.2021.09.014, Pubmed: 34901526.
20. Giuseppe, G. *et al.* Extracellular matrix hydrogel derived from decellularized tissues enables endodermal organoid culture. Nat. Commun. 11;10(1):5658 (2019).
21. Ijima, H., Nakamura, S., Bual, R. P. & Yoshida, K. Liver-specific extracellular matrix hydrogel promotes liver-specific functions of hepatocytes in vitro and survival of transplanted hepatocytes in vivo. *J. Biosci. Bioeng.* 128, 365–372 (2019). 10.1016/j.jbiosc.2019.02.014, Pubmed: 30935781.
22. Lewis, P. L. *et al.* Complex bile duct network formation within liver decellularized extracellular matrix hydrogels. *Sci. Rep.* 8, 12220 (2018). 10.1038/s41598-018-30433-6, Pubmed: 30111800.
23. Jin Won Kim *et al.* Kidney decellularized extracellular matrix enhanced the vascularization and maturation of human kidney organoids. Adv. Sci. 9, 210352 (2022).
24. Kushige, H. *et al.* Injectable extracellular matrix hydrogels contribute to native cell infiltration in a rat partial nephrectomy model. *J. Biomed. Mater. Res. B Appl. Biomater.* 111, 184–193 (2023). 10.1002/jbm.b.35144, Pubmed: 36053744.
25. Yamada, G. Histopathological characteristics and clinical significance of New Inuyama Classification in chronic hepatitis B. *Nihon Rinsho* 62 Suppl 8, 290–292 (2004). in Japanese. Pubmed: 15453332.
26. Brown, M., Li, J., Moraes, C., Tabrizian, M. & Li-Jessen, N. Y. K. Decellularized extracellular matrix: new promising and challenging biomaterials for regenerative medicine. *Biomaterials* 289, 121786 (2022). 10.1016/j.biomaterials.2022.121786, Pubmed: 36116171.
27. Kim, S. *et al.* Tissue extracellular matrix hydrogels as alternatives to Matrigel for culturing gastrointestinal organoids. *Nat. Commun.* 13, 1692 (2022). 10.1038/s41467-022-29279-4, Pubmed: 35354790.
28. Willemse, J. *et al.* Hydrogels derived from decellularized liver tissue support the growth and differentiation of cholangiocyte organoids. *Biomaterials* 284, 121473 (2022). 10.1016/j.biomaterials.2022.121473, Pubmed: 35344800.

29. Saheli, M. *et al.* Three-dimensional liver-derived extracellular matrix hydrogel promotes liver organoids function. *J. Cell. Biochem.* 119, 4320–4333 (2018). 10.1002/jcb.26622, Pubmed: 29247536.
30. Hynes, R. O. & Naba, A.. Overview of the matrisome–an inventory of extracellular matrix constituents and functions. *Cold Spring Harb. Perspect. Biol.* 4, a004903 (2012). 10.1101/cshperspect.a004903, Pubmed: 21937732.
31. Kim, S. *et al.* Tissue Extracellular Matrix Hydrogels as Alternatives to Matrigel for Culturing Gastrointestinal Organoids. Nat. Commun. 13, 1692 (2022).
32. Kikkawa, Y. *et al.* Maintenance of hepatic differentiation by hepatocyte attachment peptides derived from laminin chains. *J. Biomed. Mater. Res. A* 99, 203–210 (2011). 10.1002/jbm.a.33176, Pubmed: 21976445.
33. Pinkse, G. G. M. *et al.* Hepatocyte survival depends on beta1-integrin-mediated attachment of hepatocytes to hepatic extracellular matrix. *Liver Int.* 24, 218–226 (2004). 10.1111/j.1478-3231.2004.0914.x, Pubmed: 15189273.
34. Huang, D. *et al.* Viscoelasticity in natural tissues and engineered scaffolds for tissue reconstruction. *Acta Biomater.* 97, 74–92 (2019). 10.1016/j.actbio.2019.08.013, Pubmed: 31400521.
35. Chaudhuri, O., Cooper-White, J., Janmey, P. A., Mooney, D. J. & Shenoy, V. B. Effects of extracellular matrix viscoelasticity on cellular behaviour. *Nature* 584, 535–546 (2020). 10.1038/s41586-020-2612-2, Pubmed: 32848221.
36. Asrani, S. K., Devarbhavi, H., Eaton, J. & Kamath, P. S. Burden of liver diseases in the world. *J. Hepatol.* 70, 151–171 (2019). 10.1016/j.jhep.2018.09.014, Pubmed: 30266282.
37. Schuppan, D. & Afdhal, N. H. Liver cirrhosis. Lancet 371, 838–851 (2008). 10.1016/S0140-6736(08)60383-9.
38. Strom, S. C., Chowdhury, J. R. & Fox, I. J. Hepatocyte transplantation for the treatment of human disease. *Semin. Liver Dis.* 19, 39–48 (1999). 10.1055/s-2007-1007096, Pubmed: 10349682.
39. Lamouille, S., Xu, J. & Derynck, R. Molecular mechanisms of epithelial-mesenchymal transition. *Nat. Rev. Mol. Cell Biol.* 15, 178–196 (2014). 10.1038/nrm3758, Pubmed: 24556840.
40. Oh, S.-H., Swiderska-Syn, M., Jewell, M. L., Premont, R. T. & Diehl, A. M. Liver regeneration requires Yap1-TGFβ-dependent epithelial-mesenchymal transition in hepatocytes. *J. Hepatol.* 69, 359–367 (2018). 10.1016/j.jhep.2018.05.008, Pubmed: 29758331.
41. Pal, A., Barrett, T. F., Paolini, R., Parikh, A. & Puram, S. V. Partial EMT in head and neck cancer biology: a spectrum instead of a switch. *Oncogene* 40, 5049–5065 (2021). 10.1038/s41388-021-01868-5, Pubmed: 34239045.
42. Sun, Pingxin *et al.* Maintenance of primary hepatocyte functions in vitro by inhibiting mechanical tension-induced YAP activation. *Cell Rep.* 29, 3212–3222
.e4
(2019). 10.1016/j.celrep.2019.10.128, Pubmed: 31801084.

43. Christina, M., Tietgens, A. J. & Anderson, J. M. Visualizing the dynamic coupling of claudin strands to the actin cytoskeleton through ZO-1. *Mol. Biol. Cell.* 15 28, 524–534 (2017). 10.1091/mbc.E16-10-0698, Pubmed: 27974639.
44. Che, P., Tang, H. & Li, Q. The interaction between claudin-1 and dengue viral prM/M protein for its entry. *Virology* 446, 303–313 (2013). 10.1016/j.virol.2013.08.009, Pubmed: 24074594.
45. Bao, J. *et al.* Construction of a portal implantable functional tissue-engineered liver using perfusion-decellularized matrix and hepatocytes in rats. *Cell Transplant.* 20, 753–766 (2011). 10.3727/096368910X536572, Pubmed: 21054928.
46. Higashi, H. *et al.* Transplantation of bioengineered liver capable of extended function in a preclinical liver failure model. *Am. J. Transplant.* 22, 731–744 (2022). 10.1111/ajt.16928, Pubmed: 34932270.
47. Rouwkema, J. *et al.* Vascularization and angiogenesis in tissue engineering: beyond creating static networks. *Trends Biotechnol.* 34, 733–745 (2016). 10.1016/j.tibtech.2016.03.002, Pubmed: 27032730.
48. Yamasaki, C. *et al.* Culture density contributes to hepatic functions of fresh human hepatocytes isolated from chimeric mice with humanized livers: novel, long-term, functional two-dimensional in vitro tool for developing new drugs. *PLOS ONE* 15, e0237809 (2020). 10.1371/journal.pone.0237809, Pubmed: 32915792.
49. Mashimo, T. *et al.* Generation and characterization of severe combined immunodeficiency rats. *Cell Rep.* 2, 685–694 (2012). 10.1016/j.celrep.2012.08.009, Pubmed: 22981234.
50. Ravichandran, A., Murekatete, B., Moedder, D., Meinert, C. & Bray, L. J. Photocrosslinkable liver extracellular matrix hydrogels for the generation of 3D liver microenvironment models. *Sci. Rep.* 11, 15566 (2021). 10.1038/s41598-021-94990-z, Pubmed: 34330947.
51. Lancaster, M. A. & Knoblich, J. A. Generation of cerebral organoids from human pluripotent stem cells. *Nat. Protoc.* 9, 2329–2340 (2014). 10.1038/nprot.2014.158, Pubmed: 25188634.
52. Diehl, R. *et al.* Immunosuppression for in vivo research: state-of-the-art protocols and experimental approaches. *Cell. Mol. Immunol.* 14, 146–179 (2017). 10.1038/cmi.2016.39, Pubmed: 27721455.

Figures

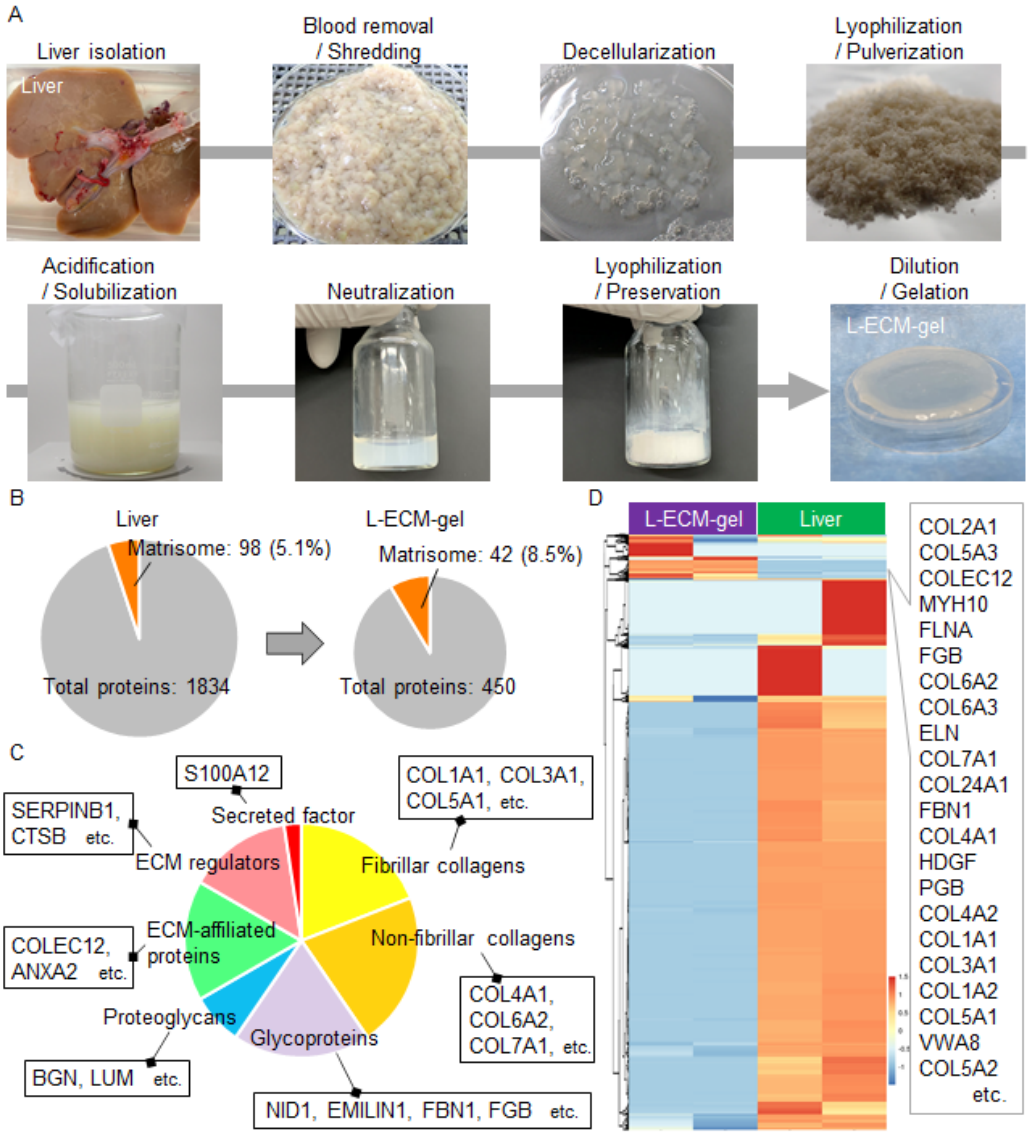

Figure 1

Figure 1

(A) Protocol for preparing decellularized liver hydrogel, and the characteristics of liver-derived extracellular matrix(L-ECM) gel. Porcine liver is minced by food dicer. This step of decellularization takes 5 days. After that, freeze drying and solubilization are performed. The appearance of pre-decellularized tissues, post-decellularized tissues, and hydrogel are shown. (B) Pie graph from the data of proteomic analysis of liver

itself and L-ECM-gel. (C) The ratio of component of matrisome in L-ECM-gel detected in proteomic analysis. (D) Hierarchical clustering analysisof matrisome compared between liver itself and L-ECM-gel.

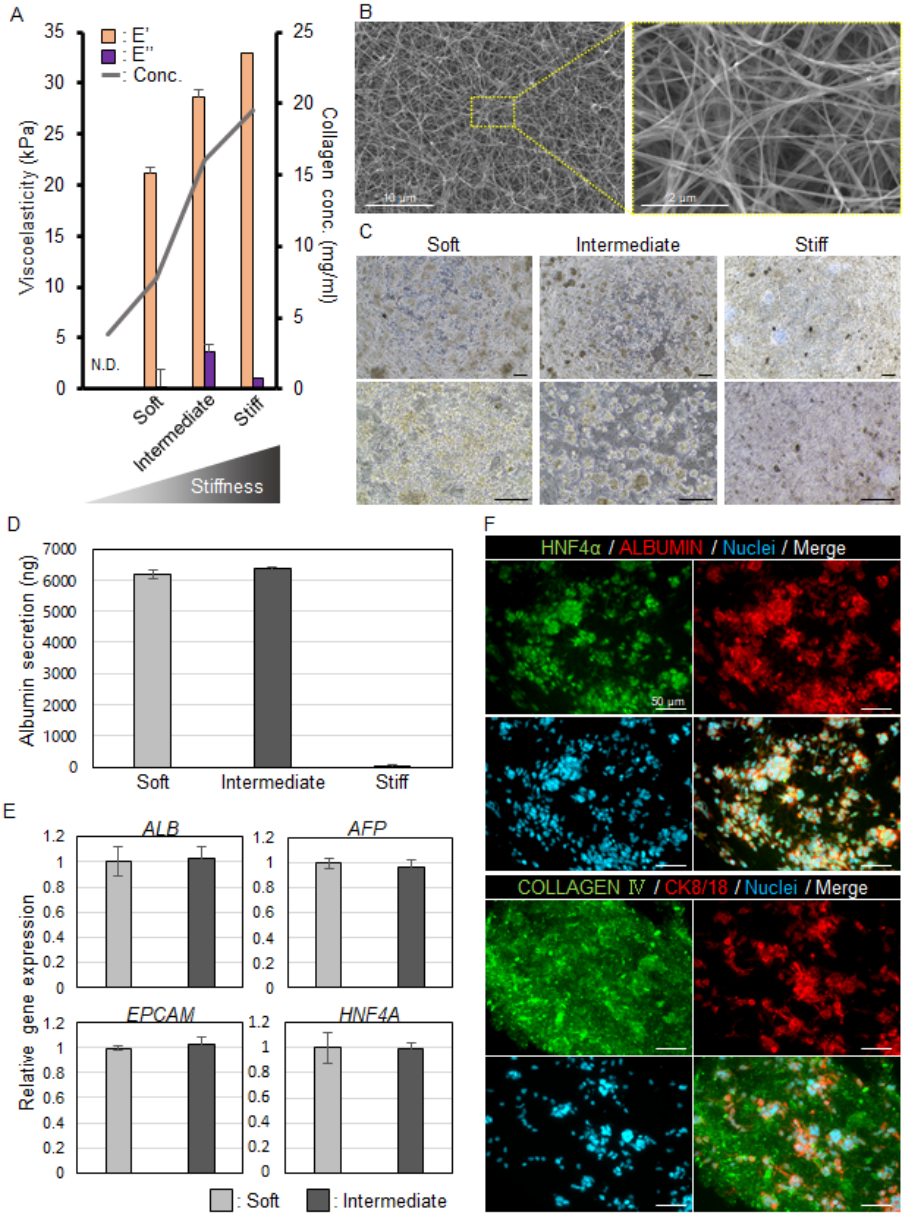

Figure 2

Figure 2

Characterization of HepG2 in L-ECM-gel according to the viscoelasticity of the L-ECM-gel. (A) The viscoelasticity of the L-ECM-gel. Ultrasoft, soft, medium, and hard was determined by complex

viscoelastic modulus (E'E" (kPa)). Collagen concentration is described as a line graph. (B) The findings of electron microscope stud of L-ECM-gel. (C) The appearance of hepatocytes (HepG2) in L-ECM-gel in vitro according to gel viscoelasticity. Scale bar, 50 μm. (D) Human albumin production of hepatocytes (HepG2) in the culture medium according to gel viscoelasticity. (E) Relative gene expression of hepatocytes (HepG2) according to gel viscoelasticity. (F) Immunostaining analysis of HepG2 encapsulated in L-ECM-gel. Scale bar, 50 μm.

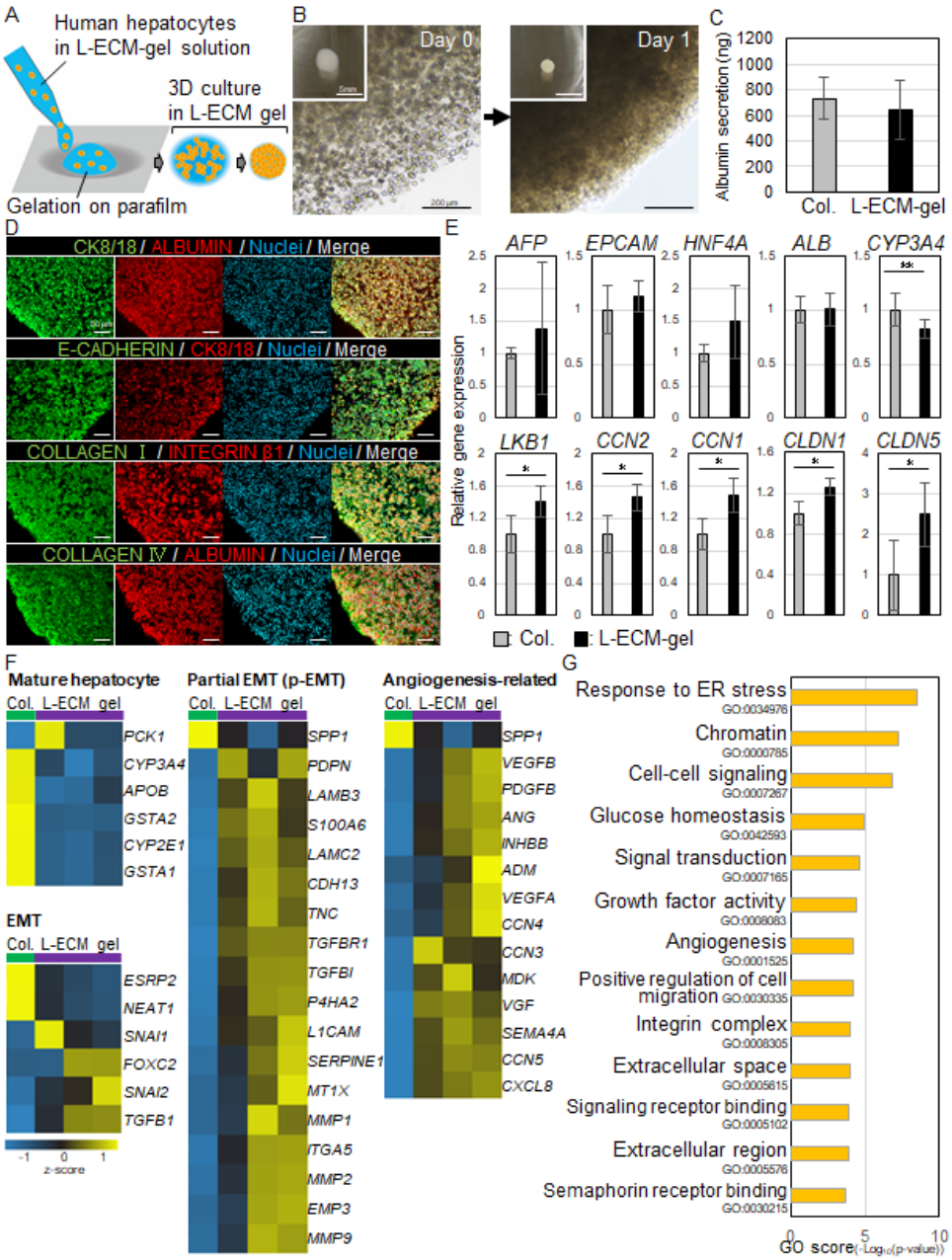

Figure 3

Figure 3

In vitro analysis of hepatocyte (PXB) function in L-ECM-gel vs. Collagen gel. (A) Scheme of in vitro analysis of hepatocyte (PXB) in L-ECM-gel. (B) The appearance of hepatocytes in vitro in L-ECM-gel on day 0 and day 1. Scale bar, 200 μm. (C) Human albumin production of hepatocytes in the culture medium. There is no statistically significant difference between PXB in L-ECM-gel and that in Collagen gel. (D) The findings of immunostaining of hepatocyte in L-ECM-gel. Scale bar, 50 μm. (E) Gene expression of hepatocytes. The expression of *AFP, ALB,* and *EPCAM* is does not exhibit statistically significant difference between hepatocytes in L-ECM-gel and that in Collagen gel. The expression of *LKB1, CLDN1,* and *CLDN4* is significantly higher in L-ECM-gel than in Collagen gel. (F) Hierarchical clustering profiles of hepatocytes encapsulated in L-ECM-gel (n=3) and collagen gel (n=1). Higher expression, relative to median expression value (black), is denoted by yellow and lower expression is denoted by blue color. (G) GO analysis of hepatocytes encapsulated in L-ECM-gel vs. collagen gel. The y axis refers to GO categories. The x axis shows GO score. * and ** means $P<0.05$, $P<0.10$, respectively.

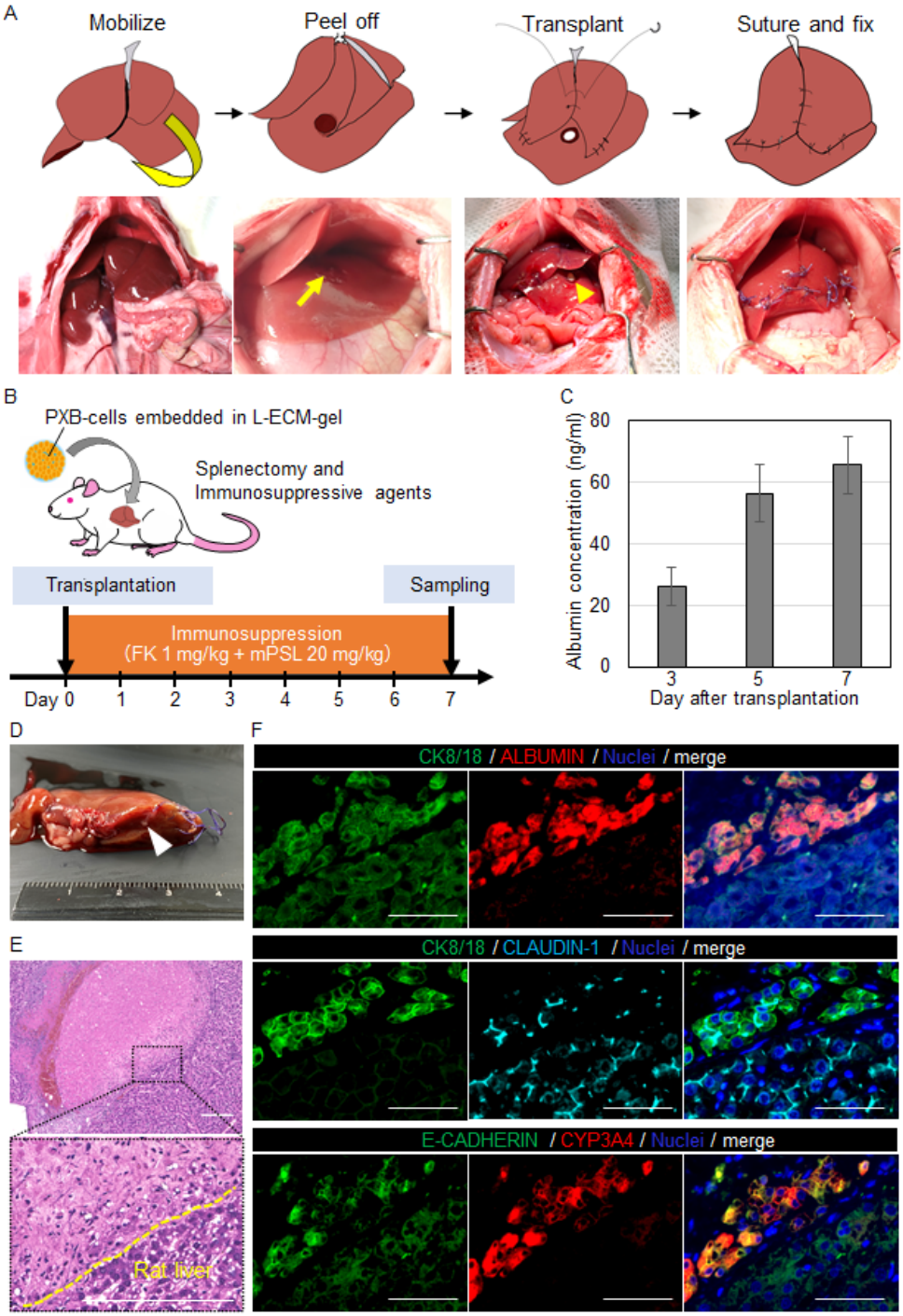

Figure 4

Figure 4

Hepatocyte (PXB) transplantation with L-ECM-gel in normal rats. (A) Scheme of the surgical procedure of hepatocyte transplantation. The peeled-off surface was expressed by arrows. (B) The protocol of immunosuppressive agents. FK, tacrolimus; mPSL, hydrocortisone sodium succinate. (C) Albumin concentration from rat blood sample on days 3, 5, and 7 after transplantation. (n=3) (D) The macroscopic, (E) HE, and immunostaining findings. L-ECM-gel was found between liver lobes (white

arrow). Cells can be found in L-ECM-gel in HE staining. (F) Immunostaining of hepatocytes in L-ECM-gel; PXB (CK8/18, Human albumin positive) expressed CYP3A4. Claudin-1 was expressed between PXB. Scale bar, 50 μm.

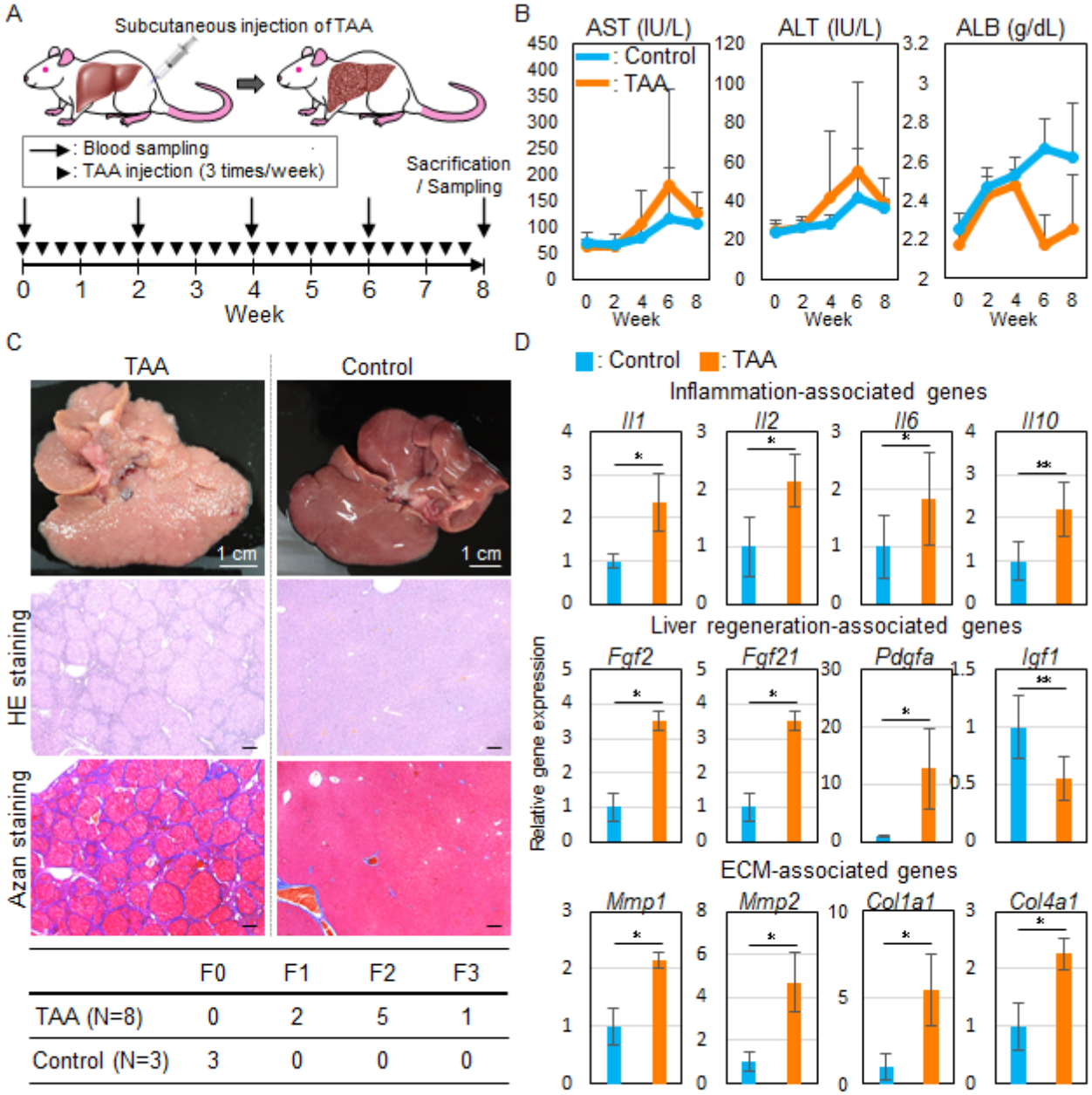

	F0	F1	F2	F3
TAA (N=8)	0	2	5	1
Control (N=3)	3	0	0	0

Figure 5

Figure 5

The rat model of drug-induced liver fibrosis using Thioacetamide (TAA). (A) The protocol of TAA admiration and blood examination. (B) The change of serum biochemical examinations of rat including ALT, AST, and albumin. There were no statistically significant differences. (C) The findings of macroscopic, HE, and Azan staining of resected liver after TAA administrations. The table below shows

the degree of liver fibrosis according to Inuyama classification. Scale bar, 1cm or 50 μm. (D) qRT-PCR of resected liver after TAA administration. The expression of MMP, Col, and Vegf was significantly elevated upon TAA administration compared with that seen in the controls. * and ** refer to P<0.05, P<0.10, respectively.

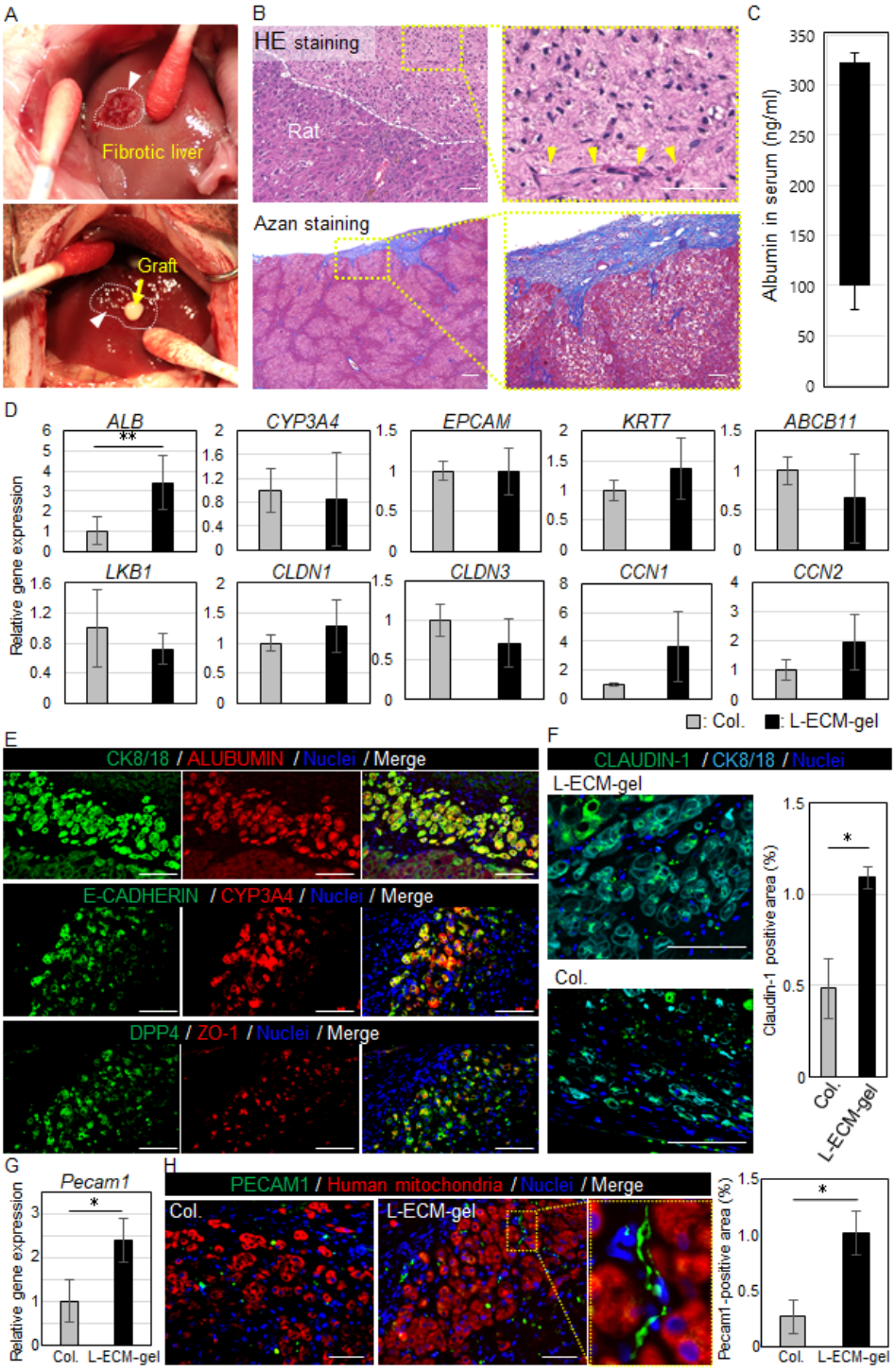

Figure 6

Figure 6

Hepatocyte (PXB) transplantation with L-ECM-gel as experiment and collagen gel as a control in drug-induced live fibrosis model of rat. (A) Photographs of transplantation. The white arrow refers to the peeled-off surface. (B) H&E staining and Azan staining of resected specimen. L-ECM-gel was observed on liver surface. In L-ECM-gel, red blood cells (yellow arrows) and nuclei cell were found. Scale bar, 50 μm. (C) Human albumin production in rat blood sample (n=3). (D) Gene expression analysis using PCR. *ALB* was significantly elevated in L-ECM-gel than in collagen gel ($P<0.05$). The expression of other genes, including *CYP3A4, EPCAM, KRT7, ABCB2, LKB1. CLDN1, CLDN2, CCN1,* and *CCN2* was similar between the two hydrogels. (E) Immunostaining of engrafted hepatocyte (CK8/18, human albumin positive). Hepatic function, CYP3A4, was expressed in hepatocytes. The tight junction marker, ZO-1 was expressed between hepatocytes. Scale bar, 50 μm. (F) The rate of claudin-1 positive area per same square measure was higher in L-ECM-gel than in collagen gel with a statistically significant difference ($p=0.024$). (G) *Pecam1* expression analysis of hepatocyte encapsulated in L-ECM-gel and collagen gel. There is a significant difference between the two hydrogels. (H) Angiogenesis in hydrogel. The rate of CD-31 positive area per graft area was higher in L-ECM-gel than in collagen gel, with a significant difference ($p=0.014$). Vascular structure was found in L-ECM-gel. Scale bar, 50 μm. * and ** refer to $P<0.05$, $P<0.10$, respectively.

Supplementary Files

This is a list of supplementary files associated with this preprint. Click to download.

- Supplementaryinformation.pdf
- Supples0423.pdf